ATF4 drives the resistance of T-ALL against FGFR1 inhibitors through amino acid metabolic reprogramming

Zijian Zhang (zhangzijian2019@wust.edu.cn)
Wuhan University of Science and Technology
Qifang Wu
Wuhan University of Science and Technology
Anqi Ren
Wuhan University of Science and Technology
Qian Chen
Wuhan University of Science and Technology
Jiangzhou Shi
Wuhan University of Science and Technology
Jiapeng Li
Wuhan University of Science and Technology
Xiyu Liu
Wuhan University of Science and Technology
Zhijie Zhang
Wuhan University of Science and Technology
Yuzhe Tang
Wuhan University of Science and Technology
Yuan Zhao
Wuhan University of Science and Technology
Ningning Yao
Peking University
Xiaoyu Zhang
Wuhan University of Science and Technology School of Medicine
Changpeng Liu
Affiliated Tumor Hospital of Zhengzhou University: Henan Cancer Hospital
Ge Dong
Wuhan University of Science and Technology
Jiaxuan Zhao
Tianjin University of Science and Technology
Meijun Xu

Wuhan University of Science and Technology
Yunqiang Yue
Wuhan University of Science and Technology
Jia Hu
Wuhan University of Science and Technology
Fan Sun
Wuhan University of Science and Technology
Yu Liu
Wuhan University of Science and Technology
Qilin Ao
Huazhong University of Science and Technology Tongji Medical College
Fuling Zhou
Zhongnan Hospital of Wuhan University
Hong Wu
Peking University
Tongcun Zhang
Wuhan University of Science and Technology
Haichuan Zhu
Wuhan University of Science and Technology

Research Article

Keywords:

Posted Date: January 4th, 2023

DOI: https://doi.org/10.21203/rs.3.rs-2415441/v1

Version of Record: A version of this preprint was published at Acta Pharmacologica Sinica on June 6th, 2023. See the published version at https://doi.org/10.1038/s41401-023-01108-4.

Abstract

Background

Abnormalities of FGFR1 have been reported in multiple malignancies, which proposes FGFR1 as a potential target for precision treatment, whereas drug resistance remains a formidable obstacle simultaneously.

Methods

RNA-seq analysis, mouse tumor models, and flow cytometry were performed to identify that the FGFR1 was a potential target in T-ALL. RNA-seq, ATAC-seq, targeted metabolomics analysis, surface sensing of translation (SUnSET) assay, western blot assays, and qRT-PCR were used to investigate the underlying mechanisms of FGFR1-targeting resistance. Drug screening was conducted to identify a drug combination strategy for overcoming this drug resistance.

Results

We identified that FGFR1 was observably upregulated in T-ALL and inversely correlated with the prognosis of patients. Functional studies showed that the knockdown of FGFR1 suppressed T-ALL cells growth and progression both *in vitro* and *in vivo*. Whereas the human T-ALL cells were resistant to FGFR1 inhibitors. Mechanistically, we identified that ATF4 was markedly upregulated and was a major initiator for T-ALL resistance to FGFR1 inhibitors. Expression of ATF4 was induced by FGFR1 inhibitors through enhancing chromatin accessibility transcriptionally combined with activating translation via the GCN2-eIF2α pathway. Then, ATF4 remodeled the amino acid metabolism by stimulating the expression of multiple metabolic genes, and further maintained the activation of mTORC1, which contributed to the drug resistance of malignancies. Moreover, targeting FGFR1 and mTOR exhibited synergistically antileukemic efficacy.

Conclusion

These findings revealed that FGFR1 was a potential therapeutic target in T-ALL, whereas ATF4-induced amino acid metabolic reprogramming mediated the FGFR1-targeted resistance. Synergistically targeting FGFR1 and mTOR could overcome this obstacle in T-ALL therapy.

Introduction

T cell acute lymphoblastic leukemia (T-ALL), a hematological malignancy deriving from T cell progenitors, accounts for about 10%-15% of pediatric and 20%-25% of adult ALL cases [1, 2]. Although the

overall survival rate with current therapeutic progress has reached 80% in pediatrics, but less than 50% in adults, the relapsed or refractory symptoms are always tough challenges for T-ALL treatment [3, 4]. Therefore, a better understanding of abnormalities and drug resistance is essential for T-ALL precision therapy.

The fibroblast growth factor receptor 1 (FGFR1), which belongs to the receptor tyrosine kinase (RTK) superfamily [5, 6], could regulate the proliferation, differentiation, and survival of cells after binding to its legends (FGFs) [7, 8]. Aberrant FGFR1 has been reported in plentiful cancers, including urothelial cancer [9], breast cancer [10], lung cancer [11], ovarian cancer [12], and Ewing sarcoma [13]. In the hematological malignancies, abnormalities of FGFR1 were described in stem cell leukemia-lymphoma syndrome (SCLL), a typical myeloproliferative disorder, which has been called myeloid/lymphoid neoplasms with eosinophilia and rearrangement of FGFR1 in the recent WHO classification [14]. These patients possibly deteriorated to B- or T-lymphoma/leukemia or AML and often with a poor prognosis [14, 15]. As described, ZNF198-FGFR1, FGFR1OP2-FGFR1 could induce myeloproliferative disorder and T-lymphoblastic leukemia in murine [16, 17]. CUX1-FGFR1 fusion was detected in T-lymphoblastic leukemia/lymphoma, which could be specifically repressed by the TKI-258, an inhibitor of receptor tyrosine kinase (RTKi) [18]. These suggested that the continuous activation of FGFR1 contributes to the formation of T cell leukemia/lymphoma and FGFR1-targeted therapy is a promising strategy for the treatment of T cell malignancies with FGFR1 aberrant.

FGFR1 inhibitors exhibited potential tumoricidal activity in multiple tumors, but the intrinsic and acquired drug resistances are also serious challenges for FGFR1-directed targeted therapy [19]. As reported, the V561M mutation, a mutation in the ATP binding site of FGFR1, could reduce the binding affinity of FGFR1 inhibitors with FGFR1 and contribute to the resistance [20]. The deletion of exon 6 in the PTEN gene was found in resistant FGFR1-driven leukemia cells, leading to the premature termination of PTEN translation and the upregulation of the PI3K-Akt signaling pathway [21]. Additionally, the activation of PUMA protein was compromised after leukemia cells acquired resistance against FGFR1 inhibitors in SCLL, which led to the incapacity of TKI-induced apoptosis [22]. However, these mechanisms could not fully encapsulate the mechanism of drug resistance, a deeper understanding is still needed.

In our study, we found that the FGFR1 was upregulated and was essential for the survival and proliferation of T-ALL cells, whereas the leukemia cells had intrinsic resistance to FGFR1 inhibitors. Mechanically, we identified that ATF4 initiated the survival-promoting amino acid metabolism reprogramming and boosted the activation of mTORC1, which contributed to drug resistance and survival. We also revealed the major causes of ATF4 upregulation in both translation and transcription levels, and further found that targeting mTORC1 could synergistically overcome the drug resistance. Briefly, we addressed the phenotypic, molecular, and metabolic response of human T-ALL cells to FGFR1 targeting, further proposed an optimal combined strategy for FGFR1-directed therapy.

Materials And Methods

Cell culture

Jurkat, NCI-H1299, SW620 and HEK-293T were purchased from the Chinese Academy of Sciences Cell Bank (CASCB, China). MOLT-3, MOLT-4, CCRF-CEM and Loucy were purchased from the American Type Tissue Culture Collection (ATCC, USA). MOLT-16 were purchased from DSMZ (Germany). Jurkat, MOLT-3, MOLT-4, CCRF-CEM, Loucy, MOLT-16, NCI-H1299 and OVCAR-8 were cultured in RPMI-1640 (Gibco, C11875500BT) with 10% FBS (Gibco, 10099-141), HEK-293T and SW620 were cultured in DMEM (Gibco, C11995500BT) with 10% FBS (Gibco, 10099-141). All of these cells were confirmed by STR profiling analysis, and were cultured in 37 ℃ cell incubator with 5% CO_2.

Gene Knockdown

The gene knockdown was performed through short hairpin RNA (shRNA) based on lentiviral vectors as described previously [23]. The sequences of shRNAs were showed in Supplementary Table 3.

Western Blot Analysis

To examine the expression and phosphorylation of specific proteins, the total proteins from different samples were used for western blot analysis as described previously [24]. Antibodies used in this study were listed in Supplementary Table 4.

Flow Cytometry

The flow cytometry protocol has been described previously [23, 25]. The cells of bone marrow were collected and washed for three times, then 1 million cells were incubated with anti-human CD7 antibody (BD Biosciences, 562635) for 30 min at 4℃. After washing three times, each sample was resuspended with PBS containing 7-AAD for dead cell exclusion. Then, the samples were detected in Beckman CytoFLEX system.

Surface Sensing Of Translation (Sunset) Assay

To examine the efficiency of protein synthesis we performed the SUnSET [26]. In brief, the samples were incubated with puromycin (10 μg/ml) for 30 min in a cell culture incubator, then were washed with PBS three times and harvested for total protein extraction. The translational efficiency was detected using an anti-puromycin antibody (1:10000), and other steps were consistent with the western blot protocol.

Rna-seq Analysis

The RNA-seq analysis has been described previously [27]. For samples preparation, Jurkat cells were transfected with FGFR1 knockdown lentivirus vectors (FGFR1-sh1, FGFR1-sh3) or non-target lentivirus vector (shC). After 36 h, treated with AZD4547 (3 μM) or PD-166866 (5 μM) or DMSO for 36 hours. Then, the total RNAs were extracted and mRNA libraries of 300–400 bp were generated with Ultima Dual-mode RNA Library Prep Kit for Illumina kit (Yeasen, 12252ES24). These libraries were performed paired-end sequencing (150 bp) using a NovaSeq 6000 platform.

Reads were aligned to the hg38 genome with STAR and protein-coding genes were calculated using R package DESeq2 [28], further to generate TPM from reads of each gene. Differentially expressed genes (DEGs) were selected with $p < 0.05$, $|\log2\ FoldChange| > 0.5$. KEGG signaling enrichment was performed by clusterProfiler [29]. Transcription factors (TFs) enrichment analysis was performed by ChEA3 with ReMap Chip-seq library [30] (https://maayanlab.cloud/chea3/). Activity analysis of transcription factors was performed by DoRothEA [31].

Atac-seq Analysis

ATAC-seq analysis has been described previously [27]. Briefly, Jurkat cells were treated with AZD4547 (2 μM) for 96 h, and generated ATAC-seq libraries with Hyperactive In-Situ ChIP Library Prep Kit for Illumina (Vazyme, TD 901) according to its protocol, then the ATAC-seq libraries were sequenced on PE150 dataset.

The clean data were generated by Trim Galore. ATAC-seq reads were aligned to the hg38 genome with Bowtie2 [32]. Then, BAM files were generated using [33], PCR duplicates were removed by Sambamba [34] and mitochondrial genomes were filtered out by Samtools [35]. Signal peaks were generated by MACS2 [36]. The motifs analysis was performed by using findMotifs.pl of Homor [37].

Targeted Metabolomics Analysis

We analyzed amino acids and their metabolites using the targeted metabolomics method. Briefly, 3 million cells were harvested and resuspended in 500 μL precooled 80% methanol/water, further suffered repeated freezing and thawing three times, the vortex was needed after thawing in each freeze-thaw cycle. The samples were centrifuged at 12000 g/min for 10 min at 4 °C, then the supernatant was collected and centrifuged again. After centrifugation, the supernatant was transferred to Protein Precipitation Plate (Thermo Scientific, 90036) preparing for further LC-MS analysis by an LC-ESI-MS/MS system (UPLC, ExionLC AD, MS, QTRAP® 6500 + LC-MS/MS) with ACQUITY BEH Amide (2.1×100 mm, 1.7 μm).

Mass spectrometric data were analyzed using Analyst and MultiQuant. The species and quantity (ng/mL) of metabolites were calculated through each standard curve, and were normalized according to their protein concentration. Differential metabolites were selected with $p < 0.05$ and $|\log2\ FoldChange| > 0.3$.

Metabolites were annotated by the KEGG compound database and mapped to the KEGG pathway database. Then the related significant pathways were identified by metabolite sets enrichment analysis (MSEA), and *p*-values were calculated by hypergeometric test.

Drug Screening

To screen the synergistic drugs with AZD4547, we screened the Approved Drug Library (TargetMol, L1000) using Jurkat cells. In brief, the 2×10^4 Jurkat cells were seeded in flat tissue culture plates (96 wells) and were treated with AZD4547 (2 μM), each drug of the library (3 μM) or combination of these two drugs for 72 hours. For the second round of screening, the combination of each drug was annotated specifically (Supplementary Table 2). The DMSO was added synchronously as the negative control. To examine the cell viability, the cells were incubated with Cell Counting Kit-8 (Yeasen, 40203ES92) following its protocol, and then detected at 450 nm (OD). The synergy of AZD4547 combined with each drug was measured by the CDI (coefficient of drug interaction), and the CDI < 1 indicated a synergistic effect [38]. Targeted pathways of each drug were annotated according to the product manual, and the first pathway was selected when the drug targeted multiple pathways. The *p*-value of pathway enrichment was calculated by the hypergeometric test.

Mouse Models

The 6 to 8-week-old NCG mice (Strain NO.T001475, NOD/ShiLtJGpt-Prkdc^{em26Cd52}Il2rg^{em26Cd22}/Gpt) were purchased from GemPharmatech (Nanjing, China). This study *in vivo* was approved by the Animal Ethics Committee of Wuhan University of Science and Technology. The protocol for Jurkat-luciferase cell-derived xenograft CDX models has been described previously [23]. CDX mice were treated with AZD4547 30 mg/kg/2 days (Aladdin, 1035270-39-3), PD-166866 30 mg/kg/2 days (MCE, HY-101296), Rapamycin 3 mg/kg/2 days (MCE, HY-10219) or combination of AZD4547 and Rapamycin intraperitoneally, PBS buffer was used as control. The progression of T-ALL was followed through imaging weekly using Imaging Systems (Spectral Instrument System, Ami HTX). The endpoint of the experiments was that weight loss exceeded 20% of the body weight of a similar normal animal according to the guidelines of the Canadian Council on Animal Care (CCAC). Then these mice were euthanized and the cells of bone marrow were collected and detected the invasion of T-ALL malignancies with anti-human CD7 antibody (BD Biosciences, 562635).

Statistics

Specific statistical analyses have been described in each section. For cell experiments, statistical significance between two groups was performed by the unpaired Student's t-test. one-way ANOVA was used to examine more than two groups. Three independent replicates have been performed unless otherwise specified, and data are represented as means ± SD. Statistical analyses were calculated using

GraphPad Prism. For clinical survival data analysis, the optimal cutoff values were determined using the maximally selected rank statistics, and the survival curves were tested with the log-rank test.

Results

FGFR1 is upregulated in T-ALL and associated with dismal prognosis in patients

To identify potential targets for the treatment of T-ALL, we analyzed gene expression profiles of our previous T-ALL cohort [39] and another T-ALL RNA-seq dataset [40], and identified 226 genes and 264 genes that were upregulated in T-ALL respectively (Fig. 1a and Supplementary Fig. 1a). 35 common genes were shared by both upregulated groups, several of which were involved in the progression of T-ALL as previous reported, such as STMN1, CD99, SOX4, MYB, CDK6 and TOX (Supplementary Fig. 1b). However, the functional roles of FGFR1, one of the significantly upregulated 35 genes, remains largely unclear in T-ALL. (Fig. 1b, c). We detected the expression of the FGFR family (FGFR1-4) in T-ALL and found that only FGFR1 was expressed in T-ALL (Supplementary Fig. 1c).

Next, we confirmed that FGFR1 was upregulated in T-ALL cell lines and primary T-ALL blasts compared to normal T cells at both transcription and translation levels (Fig. 1d, e). Since the upregulation of FGFR1 has been reported in numerous malignancies [41], we summarized the transcription level of FGFR1 in various types of leukemia or lymphoma through the Cancer Cell Line Encyclopedia database (CCLE), and revealed that the FGFR1 was highest expressed in T-ALL compared with other hematopoietic malignancies (Fig. 1f). Subsequently, we identified that the expression of FGFR1 in relapsed T-ALL samples was not significantly reduced compared to the primary T-ALL blasts (Supplementary Fig. 1d), indicating that the FGFR1-directed therapy also has therapeutic potential in relapsed T-ALL patients. Importantly, T-ALL patients with higher FGFR1 expression were more prone to relapse or other adverse events and had shorter survival time than patients with lower FGFR1 expression (TARGET, phs000464) (Fig. 1g, h). The comparable results were observed in a B-ALL cohort (TARGET, phs000463) (Supplementary Fig. 1e, f). Taken together, FGFR1 was substantially elevated in T-ALL and negatively related to the prognosis of the T-ALL patients.

FGFR1 is a potential therapeutic target in T-ALL but leukemia cells are resistant to FGFR1 inhibitors

Next, we examined the functional roles of FGFR1 in T-ALL. After silencing the FGFR1 in human T-ALL cell lines through RNA interference, the proliferation and survival of T-ALL cells were impaired observably (Fig. 2a-d). Then, we inhibited the function of FGFR1 through its inhibitors, and found that all T-ALL cell lines were insensitive to FGFR1 inhibitor AZD4547 (IC50 > 3 μM) and did not even respond to another FGFR1 inhibitor PD-166866 compared to normal T cells (low FGFR1 expression) (Fig. 1e, f). To further evaluate the anti-T-ALL efficiency of blocking FGFR1 *in vivo*, we established cell-derived xenograft (CDX) based on fluorescence-labeled Jurkat or FGFR1-knockdown Jurkat cells, As the schematic diagram showing, AZD4547 (30 mg/kg/2 days) or PD-166866 (30 mg/kg/2 days) was administrated from day 14

to day 28 (Fig. 2g). Both AZD4547 and PD-166866 did not suppress the growth of human T-ALL cells, while the FGFR1 knockdown significantly inhibited the progression of T-ALL cells *in vivo* (Fig. 2h, i). Similarly, the survival time of mice was extended in the FGFR1 knockdown group, but not in the AZD4547 or PD-166866 treatment groups (Fig. 2j). We also analyzed the bone marrow invasion in CDX through flow cytometry analysis, and found that both of the FGFR1 inhibitors could not significantly prevent the leukemia cells invading to bone marrow compared to FGFR1 knockdown group (Fig. 2k, l). Together, FGFR1 was essential for T-ALL progression but the leukemia cells were resistant to FGFR1 inhibitors.

Atf4 Is Essential For The Resistance Against Fgfr1 Inhibitors

To comprehend the mechanism under the resistance of T-ALL cells against FGFR1 inhibitors, we performed RNA-seq in Jurkat cells after FGFR1 knockdown or treatment with FGFR1 inhibitors. The differentially expressed genes (DEGs) compared with the control group were summarized in the heatmap, and the DEGs were similar between AZD4547 and PD-166866 treatment groups (Fig. 3a). Only 28 DEGs co-changed in all three groups, while 598 common DEGs were shared in FGFR1 inhibitors treated groups (Fig. 3b), suggesting that the 570 DEGs had potential relevance to the FGFR1 inhibitors resistance. These 570 DEGs were significantly enriched in several pathways about survival-promoting metabolism, including amino acid metabolism, carbon metabolism and glucose, and fructose metabolism (Fig. 3c). Whereas, the pathways enriched of the DEGs in FGFR1 knockdown group were the transcriptional misregulation in cancer and FoxO signaling pathway, which were related to gene expression and cell fate decisions [42, 43], which were dramatically different from those pathways in the groups of FGFR1 inhibitors (Supplementary Fig. 2a).

To enquire whether there was a sponsor gene to drive these transformations of 570 DEGs, we analyzed the upstream transcription factors (TFs) through ChEA3 [30]. Among the predicted TFs, ATF4 scored the highest with the minimum *p*-value (1.82×10^{-16}) and maximum genes coverage (Fig. 3d). However, the TFs enriched by DEGs in FGFR1 knockdown group were obviously distinct (Supplementary Fig. 2b). We also examined the Transcripts Per Million (TPM) of ATF4 in different groups of RNA-seq and found that the ATF4 highly increased in both AZD4547 and PD-166866 treatment groups, while not in FGFR1 knockdown group (Fig. 3e). The transcription and protein levels of ATF4 was gradually increased over time after AZD4547 and PD-166866 treatment in human T-ALL cell lines (Fig. 3f-h). However, we found that ATF4 did not elevate in FGFR1 knockdown Jurkat cells, indicating that the upregulated of ATF4 was not due to functional deficiency of FGFR1 (Fig. 3i). The Jurkat cells were more sensitive to AZD4547 after ATF4 knockdown compared with the control group (Fig. 3j). To amplify the feature and make it feasible to identify critical factors of drug resistance, we further developed a more resistant Jurkat cell line (Jurkat-AZD) through continuously exposing to AZD4547 for a long time (Supplementary Fig. 2c, d). Consistently, the Jurkat-AZD cells became less resistant to AZD4547 after ATF4 knockdown (Fig. 3k). These results indicated that ATF4 was important for the resistance to FGFR1 inhibitors in T-ALL cells.

Atf4 Is Induced By Enhanced Chromatin Accessibility Combined With Gcn2-mediated Translational Activation

To investigate the molecular mechanism behind ATF4 upregulation after FGFR1 inhibitors treatment, we performed ATAC-seq with high spatial resolution. Overall, the average ATAC-seq signal around the transcription start sites (TSSs) was increased after AZD4547 treatment (Fig. 4a, b). The distribution of the average ATAC-seq signal in different regions also changed, especially increased in the regions of promotors (Fig. 4c). We identified the significant active TFs (top 20) based on RNA-seq data (Fig. 4d), and screened the motifs of transcription factors that significantly enriched in the regions of promotors by ATAC-seq data synchronously (Fig. 4e). Together with 570 DEGs in both FGFR1 inhibitors groups, we found that only two common TFs were shared in all three groups, one was ATF4 (Fig. 4f). These results were consistent with our above data that ATF4 was at the vital place for initiating these transcriptional changes. Subsequently, we examined the change in the ATF4 promotor region and found the chromatin accessibility was enhanced after AZD4547 treatment (Fig. 4g), as well as in the promotor region of ASNS, which was the direct target gene of ATF4 (Fig. 4h). These data indicated that increased chromatin accessibility in its promotor region was a potential cause of the transcriptional upregulation of ATF4.

The translation of ATF4 could be induced by eIF2α through integrated stress response (ISR) when cells suffered multiple survival pressures [44]. Amino acid deprivation and endoplasmic reticulum (ER) stress could activate eIF2α through GCN2 and PERK respectively, which were closely related to amino acid metabolism and proteostasis [45]. Here, we examined the possible involvement of these stress-related kinases in the initiation of ATF4 translation. Based on 570 DEGs from RNA-seq, we observed that the amino acid deprivation pathway was highly enriched, which is closely related to the GCN2 kinase (Fig. 4i). The increase of ATF4 was ceased after GCN2 knockdown (Fig. 4j), but not entirely suppressed after PERK knockdown (Fig. 4k). We further functionally determined the role of GCN2 in drug resistance, found that Jurkat cells were more sensitive to AZD4547 with GCN2 knockdown (Fig. 4l), but not with PERK knockdown (Data not shown). Similar results were obtained when we combined AZD4547 with SP600125 (a GCN2 inhibitor) [46, 47] (Fig. 4m). These results indicated that the translational upregulation of ATF4 mediated by AZD4547 was mainly due to GCN2-eIF2α pathway.

Atf4 Is A Crucial Initiator To Drive The Reprogramming Of Amino Acid Metabolism

We have indicated that the DEGs in the groups of FGFR1 inhibitors were enriched in metabolic pathways (Fig. 3c) and identified that the ATF4 was the initiator of these transformations (Fig. 3d and Fig. 4f). We further identified that these typical DEGs mainly divided into three categories, including kinases about metabolism, transporter, and aminoacyl-tRNA biosynthesis, and all of these DEGs were significantly elevated in both groups of FGFR1 inhibitors (Fig. 5a). mRNA levels of these typical genes were dramatically increased, and chromatin accessibility around some of these genes was enhanced after AZD4547 treatment (Supplementary Fig. 3a-d). The upregulated expression of mRNAs was blocked after

knockdown of ATF4 (Fig. 5b-d). Next, we selected several typical genes to confirm the tendencies in the protein levels, and found that the protein levels of ASNS, ASS1, PHGDH, and SLC1A5 were significantly increased, with the protein of ATF4 increasing ahead of these proteins (Fig. 5e), Besides, these upregulations of proteins were similar in the more resistant Jurkat cells (Jurkat-AZD) (Fig. 5f). These AZD4547 induced upregulations were also interdicted after ATF4 knockdown (Fig. 5g). Together, the upregulations of these metabolic genes were induced by ATF4 when cells exposed to FGFR1 inhibitors.

Since these typical DEGs had relevance to amino acid biosynthesis and uptake, we next quantified the intracellular amino acids and their metabolites through the targeted metabolomics analysis (Supplementary Table 1). Plentiful amino acids and metabolites significantly increased in the more resistant Jurkat cells (Jurkat-AZD) and came down after ATF4 knockdown. Especially, Asn, Arg and other essential amino acids (EAAs) that were related to ASNS, ASS1, and SLC1A5 (Fig. 5h and Supplementary Fig. 3e). Subsequently, we systematically revealed that these differential amino acids, and found these differential metabolites were mainly enriched in the pathways about central carbon metabolism (related to PHGDH [48]), alanine/aspartate/glutamate/glycine/serine/ threonine metabolism, mineral absorption and TCA cycle, all of which were essential for cell survival and proliferation [49]. Importantly, these metabolic pathways were enhanced in the more resistant Jurkat cells (Jurkat-AZD) and fell back after ATF4 knockdown (Fig. 5h), suggesting that ATF4 upregulated the intracellular quantities of amino acids under FGFR1 inhibitor treatment.

Targeting Mtor Could Overcome The Resistance Against Fgfr1 Inhibitors

To investigate the strategy of concomitant medications to overcome this resistance therapeutically, we performed drug screening (2059 approved drugs). After two rounds of screening, 30 drugs that had synergistic effects with AZD4547 were identified with the coefficient of drug interaction (CDI) < 1 [38] (Fig. 6a, Supplementary Table 2). The targets of these drugs were significantly enriched in angiogenesis and PI3K/Akt/mTOR signaling (Fig. 6b). Since the PI3K/Akt/mTOR pathway was relevant to amino acid metabolism [50], we focused on this pathway and found all of these three drugs (Temsirolimus, Rapamycin, and Zotarolimus) were the inhibitors of mTOR (Fig. 6c).

After further verification, we found that the combination of Rapamycin and AZD4547 could significantly inhibit the viability of T-ALL cells, including Jurkat (CDI minimum = 0.12), MOLT-4 (CDI minimum = 0.35) and MOLT-16 (CDI minimum = 0.45) (Fig. 6d and Supplementary Fig. 4a, b). However, PKI-587, a PI3K inhibitor, did not exhibit obvious synergy with AZD4547 (Supplementary Fig. 4c), indicating that the mTOR pathway, not the PI3K/AKT pathway, contributed to the FGFR1 drug resistance. We also found that the Jurkat-AZD cells were more sensitive to Rapamycin (Fig. 6e). These results indicated that mTOR was an indispensable effector for drug resistance, and the resistance to FGFR1 inhibitors could enhance the sensibility of cells to Rapamycin. We further found that ATF4 was induced by FGFR1 inhibitors in other FGFR1-upregulated malignancies, such as NCI-H1299 (NSCLC), OVCAR-8 (ovarian cancer), and SW620

(colorectal cancer) cells (Supplementary Fig. 4d, e), and the strategy of concomitant drugs was also applicable to these cell lines (Supplementary Fig. 4f-h). These suggested that the resistance to FGFR1 inhibitors mediated by ATF4 was universal and that targeting mTOR could overcome this resistance synergistically.

To further confirm the synergistic effect *in vivo*, we established the Jurkat-luci cell-derived xenograft mouse models (CDX). AZD4547 (30 mg/kg/2 days), Rapamycin (3 mg/kg/2 days) or the combination of these two drugs were administrated from day 17 to 29 intraperitoneally (Fig. 6f). The T-ALL progression in the combination group was significantly inhibited compared with other groups (Fig. 6g, h). The combination of AZD4547 and Rapamycin prolonged the survival time of the CDX (Fig. 6i), and significantly reduced the bone marrow invasion of T-ALL cells (Fig. 6j, k). Together, our data indicated that synergistically targeting FGFR1 and mTOR could inhibit the progression of T-ALL cells *in vitro* and *in vivo*.

Reprogramming Of Amino Acid Metabolism Induces The Activation Of Mtorc1

The synergistic effect of AZD4547 and Rapamycin suggested that there might exist a compensatory activation of mTOR. We further monitored the phosphorylation ribosome protein S6 (p-S6), a reliable marker of mTORC1 activation, for a long time with AZD4547 treatment. The phosphorylation of S6 was decreased in the first few days, but restored after a long time under AZD4547 treatment (Fig. 7a). We further used the more resistant Jurkat cells (Jurkat-AZD) to amplify the feature of drug resistance and identified the crucial factors, found that the phosphorylation of S6 did not reduce in the more resistant Jurkat cells (Jurkat-AZD) compared to Jurkat cells under AZD4547 treatment (Fig. 7b). Since the ribosome protein S6 is involved with translation, we also found of translational efficiency of total proteins was impaired in Jurkat cells, but did not decrease in the more resistant Jurkat cells (Jurkat-AZD) (Supplementary Fig. 5a, b). These results highlighted that the compensatory activation of mTORC1 was essential for the resistance to FGFR1 inhibitors.

To explore the connection between amino acid metabolism and the activation of mTORC1, we knockdown the ATF4 in the more resistant Jurkat cells (Jurkat-AZD), which had high ATF4 expression, found the phosphorylation of S6 and typical proteins (ASNS, ASS1, SLC1A5, and PHGDH) were significantly reduced (Fig. 7c). The translational efficiency was dramatically reduced after ATF4 knockdown in both cell lines (Supplementary Fig. 5c). Importantly, we found the phosphorylation of S6 was significantly decreased after knockdown of ASNS, ASS1, SLC1A5, and PHGDH respectively. The Jurkat-AZD cells became more sensitive to AZD4547 and PD-166866 (Fig. 7d-g and Supplementary Fig. 5d-g). In summary, the reprogramming of amino acid metabolism induced the activation of mTORC1 and further contributed to resistance against FGFR1 inhibitors.

Discussion

Targeting FGFR signaling by tyrosine kinase inhibitors (TKIs) was a successful therapeutic strategy in numerous tumors with FGFR abnormalities [51]. Three FGFRs inhibitors that applied for mutations or translocations of FGFR2 or FGFR3 have been approved for urothelial cancer or cholangiocarcinoma [52–54]. However, no inhibitor applied to any type of aberrations of FGFR1 was approved, though the FGFR1 aberrations make up 49% of all abnormalities of the FGFR family [41]. Due to drug resistance, only about 11% of FGFR1-amplified tumors respond to FGFR1 inhibitors, several malignancies exhibited insufficient tumor shrinkage [55]. In our manuscript, we identified that the FGFR1 was significantly upregulated in T-ALL and was negatively related to the prognosis of the patients (Fig. 1 and Supplementary Fig. 1). We further confirmed that FGFR1 was essential for T-ALL progression, and was a promising target for T-ALL therapy. However, both FGFR1 inhibitors AZD4547 and PD166866 did not exhibit antileukemic efficacy in T-ALL treatment, though AZD4547 had reached phase II clinical investigations (Fig. 2), suggesting that T-ALL malignancies carrying FGFR1 overexpression have intrinsic resistance to FGFR1 inhibitors. Further, our results addressed the detailed mechanism of the drug resistance to FGFR1 inhibitors and provide a potential avenue to overcome the obstacle in malignancies with FGFR1 overexpression.

ATF4 is a core stress-induced transcription factor of the integrated stress response (ISR), which is important for metabolic, and redox processes and could adapt cells to adverse stresses, including proteostasis defects, nutrient deprivation, viral infection and redox imbalances [44, 56]. Previous studies showed that ATF4 could drive resistance to sorafenib by preventing ferroptosis and resistance to gemcitabine via the TGF-beta1/SMAD2/3 pathway [57, 58]. Here, we identified that the ATF4 was significantly increased during FGFR1 inhibitors treatment and was essential for the resistance to FGFR1 inhibitors (Fig. 3). Under a variety of stress conditions, the translational of ATF4 was activated by p-eIF2α mainly through four kinases, including GCN2, PERK, PKR, and HRI. Especially, the GCN2 and PERK were closely related to amino acid and protein metabolism [59, 60]. Here, we found that the translational upregulation of ATF4 was mainly dependent on the GCN2-eIF2α pathway under FGFR1 inhibitors treatment (Fig .4). Besides, the mRNA of ATF4 was dramatically increased after treatment with FGFR1 inhibitors. Since the mRNA transcription was closely related to transposase accessibility [61], we performed ATAC-seq to describe the transposase accessibility in whole chromatin. The average transposase accessibility was increased in the regions of total promotors especially in the promotor of ATF4 after exposure to FGFR1 inhibitors, which contribute to the transcriptional upregulation of ATF4 appropriately (Fig. 4). There results elaborated the mechanism about the upregulation of ATF4 in both transcription and translation levels.

Amino acid metabolism was closely related to the survival and progression of malignancies [62, 63]. ASNS mediated the resistance of leukemia to L-asparaginase by regulating Asparagine synthesis [64]. SLC1A5 contributed to the resistance of Apatinib in non-small-cell lung cancer through the reprogramming of glutamine metabolism [65]. Here, we found that many survival-promoting metabolisms, especially the amino acid metabolism and its metabolites, were upregulated after FGFR1 inhibitors treatment (Fig. 3, 5 and Supplementary Fig. 3). More importantly, we identified that ATF4 was the sponsor of these transformations. These upregulations of survival-promoting metabolisms were interrupted after ATF4

knockdown, which revealed the initiator role of ATF4 in these metabolic processes, and also provided a promising strategy for targeted therapy. Though blocking TFs remains challenges in terms of treatment, the success of DB1976, a PU.1 inhibitor that could competitively block with the motif of PU.1, suggested that a fresh idea for ATF4-targeted therapy to overcome the FGFR1 inhibitor resistance [66].

Drug screening is the process of identifying and optimizing prospective medications in high-throughput assays, which is also used to screen a specific biological function [67]. To identify the main effectors that mediated T-ALL cells resisting FGFR1 inhibitors and find out a synergistic strategy on the treatment side, we screened the approved drug library, which comprises 2059 approved drugs for clinical treatment. We further identified that combined targeting mTORC1 and FGFR1 significantly inhibited the survival and proliferation of T-ALL cells, and the compensatory activation of mTORC1 contributed to the drug resistance (Fig. 6, 7 and Supplementary Fig. 4). Interestingly, our previous study revealed that the T-ALL were resistant to the single rapamycin treatment, especially in the T-ALL leukemia stem cells [25], and the essential role of FGFR1 in stem cell leukemia [68]. It is worth trying FGFR1 inhibitors combined with rapamycin for leukemia stem cell debulking.

The mTORC1 is a master regulator that couples amino acid availability to cell survival, growth and drug resistance. Multiple factors modulate mTORC1 activity, such as growth factors, stress, energy status, and amino acids [50, 69]. Here, we revealed that inhibiting the pivotal metabolic processes through knockdown of the key kinases (ASNS, ASS1, SLC1A5, and PHGDH) could directly inhibit mTORC1 activity and enhance susceptibility to FGFR1 inhibitors (Fig. 7 and Supplementary Fig. 5). As previously stated, the increase of Arg, Asn, and other EAAs could boost the mTORC1 activation [70–73]. These findings implied that the upregulated amino acid biosynthesis and EAA uptake mediated by ATF4 were essential for mTORC1 activation and the resistance to FGFR1 inhibitors. Moreover, these results also suggested that blocking ASNS, ASS1, SLC1A5 or PHGDH were promising solutions for drug resistance, which needed further confirmation

Besides, several types of immunotherapies, including antibody therapy and CAR T cell therapy, have achieved durable clinical responses by targeting tumor-associated antigens [74, 75]. We had successful cases that targeted CD99 or CD30 to eliminate T-ALL or Hodgkin lymphoma respectively [23, 76]. Since FGFR1 is a membrane protein and upregulated in T-ALL compared with very low expression levels in normal T cells, it is possible to try chimeric antigen receptors (CAR) based immunotherapy. In summary, our study identified the pivotal role of FGFR1 in T-ALL survival and proliferation, elucidated the mechanism of resistance to FGFR1 inhibitors, and proposed potential approaches of concomitant drugs for FGFR1-directed therapy in T-ALL.

Declarations

Acknowledgments

We are obliged to Jian Lin, Long Chen (College of Chemistry and Molecular Engineering, Peking University), Hudan Liu (Medical Research Institute, Wuhan University), and Yuan Cao, Piao Zou (Analytical & Testing Center, Wuhan University of Science and Technology) for their assistance in the experiments.

Authors' contributions

H.Z., Z.Z. and T.Z. designed the experimental plans; Z.Z., A.R., J.S., J.L., X.L., Z.Z., Y.T., Y.Z., N.Y., X.Z., C.L., G.D., J.Z., M.X, and Y.Y. performed the experiments. Q.W., and Q.C. performed the bioinformatic analysis. Z.Z., and H.Z. analyzed the data and drafted the manuscript. F.S., Y.L., J.H., Q.A., F.Z., and H.W. were involved in the revision of the manuscript.

Funding

This work was funded by the grants from the Wuhan Science and Technology Plan Project (2019030703011533) to Tongcun Zhang, China Postdoctoral Science Foundation (2021M702538), Department of Education of Hubei Province (B2021023), and National Natural Science Foundation of China (82203497) to Jiapeng Li, and also supported by China Postdoctoral Science Foundation (2020M682491), Wuhan former funded science and technology program (2020020602012111), grand science and technology special project carried out by the Department of Science and Technology of Hubei Province (2020BCB048), and National Natural Science Foundation of China (82100193) to Haichuan Zhu.

Availability of data and materials

The sequence data of RNA-seq and ATAC-seq reported in this study have been deposited in the Genome Sequence Archive (GSA) for human under accession number HRA004859 and HRA004864 respectively. Other published data used in this paper were listed as follows: RNA-seq data of T-ALL cohorts were from Genome Sequence Archive (GSA) for human (HRA000122), Gene Expression Omnibus (GEO) (GSE26713), and database of genotypes and phenotypes (TARGET, phs000464). RNA-seq data about a primary and relapse T-ALL cohort were from NCBI BioProject (PRJNA534488). Survival data of T-ALL were from TARGET, phs000464, and of B-ALL were from TARGET, phs000463. H3K27ac ChIP-seq of Jurkat cells was from Gene Expression Omnibus (GEO), GSE68978. H3K4me3 ChIP-seq of Jurkat cells was from Gene Expression Omnibus (GEO), GSE151297. Data related to this paper may be requested from the corresponding author.

Ethical approval and consent to participate

All experiments were approved by the College of Life Sciences and Health, Wuhan University of Science and Technology. In vivo experiments were approved by the Animal Ethics Committee of Wuhan University of Science and Technology.

Consent for publication

All authors have read and agreed to the published version of the manuscript.

Competing interests

The authors declare that they have no conflict of interest.

References

1. Dores GM, Devesa SS, Curtis RE, Linet MS, Morton LM. Acute leukemia incidence and patient survival among children and adults in the United States, 2001–2007. Blood 2012 Jan 5; **119**(1): 34–43.
2. Pui CH, Mullighan CG, Evans WE, Relling MV. Pediatric acute lymphoblastic leukemia: where are we going and how do we get there? Blood 2012 Aug 9; **120**(6): 1165–1174.
3. Patrick K, Wade R, Goulden N, Mitchell C, Moorman AV, Rowntree C, et al. Outcome for children and young people with Early T-cell precursor acute lymphoblastic leukaemia treated on a contemporary protocol, UKALL 2003. Br J Haematol. 2014 Aug;166(3):421–4.
4. Winter SS, Dunsmore KP, Devidas M, Wood BL, Esiashvili N, Chen Z, et al. Improved Survival for Children and Young Adults With T-Lineage Acute Lymphoblastic Leukemia: Results From the Children's Oncology Group AALL0434 Methotrexate Randomization. J Clin Oncol. 2018 Oct;10(29):2926–34. ; **36**.
5. Katoh M, Nakagama H. FGF receptors: cancer biology and therapeutics. Med Res Rev. 2014 Mar;34(2):280–300.
6. Turner N, Grose R. Fibroblast growth factor signalling: from development to cancer. Nat Rev Cancer. 2010 Feb;10(2):116–29.
7. Eswarakumar VP, Lax I, Schlessinger J. Cellular signaling by fibroblast growth factor receptors. Cytokine Growth Factor Rev. 2005 Apr;16(2):139–49.
8. Katoh M. Therapeutics Targeting FGF. Signaling Network in Human Diseases. Trends Pharmacol Sci. 2016 Dec;37(12):1081–96.
9. Knowles MA, Hurst CD. Molecular biology of bladder cancer: new insights into pathogenesis and clinical diversity. Nat Rev Cancer. 2015 Jan;15(1):25–41.
10. Elbauomy Elsheikh S, Green AR, Lambros MB, Turner NC, Grainge MJ, Powe D, et al. FGFR1 amplification in breast carcinomas: a chromogenic in situ hybridisation analysis. Breast Cancer Res. 2007;9(2):R23.
11. Kim HR, Kim DJ, Kang DR, Lee JG, Lim SM, Lee CY, et al. Fibroblast growth factor receptor 1 gene amplification is associated with poor survival and cigarette smoking dosage in patients with resected squamous cell lung cancer. J Clin Oncol. 2013 Feb;20(6):731–7. ; **31**.
12. Xiao H, Wang K, Li D, Wang K, Yu M. Evaluation of FGFR1 as a diagnostic biomarker for ovarian cancer using TCGA and GEO datasets. PeerJ. 2021;9:e10817.
13. Agelopoulos K, Richter GH, Schmidt E, Dirksen U, von Heyking K, Moser B, et al. Deep Sequencing in Conjunction with Expression and Functional Analyses Reveals Activation of FGFR1 in Ewing

Sarcoma. Clin Cancer Res. 2015 Nov;1(21):4935–46. ; **21**.

14. Arber DA, Orazi A, Hasserjian R, Thiele J, Borowitz MJ, Le Beau MM, et al The 2016 revision to the World Health Organization classification of myeloid neoplasms and acute leukemia. Blood 2016 May 19; **127**(20): 2391–2405.
15. Jackson CC, Medeiros LJ, Miranda RN. 8p11 myeloproliferative syndrome: a review. Hum Pathol 2010 Apr; 41(4): 461–476.
16. Qin H, Wu Q, Cowell JK, Ren M. FGFR1OP2-FGFR1 induced myeloid leukemia and T-cell lymphoma in a mouse model. Haematologica 2016 Mar; 101(3): e91-94.
17. Ren M, Li X, Cowell JK. Genetic fingerprinting of the development and progression of T-cell lymphoma in a murine model of atypical myeloproliferative disorder initiated by the ZNF198-fibroblast growth factor receptor-1 chimeric tyrosine kinase. Blood 2009 Aug 20; **114**(8): 1576–1584.
18. Wasag B, Lierman E, Meeus P, Cools J, Vandenberghe P. The kinase inhibitor TKI258 is active against the novel CUX1-FGFR1 fusion detected in a patient with T-lymphoblastic leukemia/lymphoma and t(7;8)(q22;p11). Haematologica. 2011 Jun;96(6):922–6.
19. Krook MA, Reeser JW, Ernst G, Barker H, Wilberding M, Li G, et al. Fibroblast growth factor receptors in cancer: genetic alterations, diagnostics, therapeutic targets and mechanisms of resistance. Br J Cancer. 2021 Mar;124(5):880–92.
20. Sohl CD, Ryan MR, Luo B, Frey KM, Anderson KS. Illuminating the molecular mechanisms of tyrosine kinase inhibitor resistance for the FGFR1 gatekeeper mutation: the Achilles' heel of targeted therapy. ACS Chem Biol. 2015 May;15(5):1319–29.. ; **10**.
21. Cowell JK, Qin H, Hu T, Wu Q, Bhole A, Ren M. Mutation in the FGFR1 tyrosine kinase domain or inactivation of PTEN is associated with acquired resistance to FGFR inhibitors in FGFR1-driven leukemia/lymphomas. Int J Cancer 2017 Nov 1; **141**(9): 1822–1829.
22. Liu Y, Cai B, Chong Y, Zhang H, Kemp CA, Lu S, et al. Downregulation of PUMA underlies resistance to FGFR1 inhibitors in the stem cell leukemia/lymphoma syndrome. Cell Death Dis. 2020 Oct;20(10):884. ; **11**.
23. Shi J, Zhang Z, Cen H, Wu H, Zhang S, Liu J, et al. CAR T cells targeting CD99 as an approach to eradicate T-cell acute lymphoblastic leukemia without normal blood cells toxicity. J Hematol Oncol. 2021 Oct;9(1):162. ; **14**.
24. Schubbert S, Cardenas A, Chen H, Garcia C, Guo W, Bradner J, et al Targeting the MYC and PI3K pathways eliminates leukemia-initiating cells in T-cell acute lymphoblastic leukemia. Cancer Res 2014 Dec 1; **74**(23): 7048–7059.
25. Zhu H, Zhang L, Wu Y, Dong B, Guo W, Wang M, *et al.* T-ALL leukemia stem cell 'stemness' is epigenetically controlled by the master regulator SPI1. *Elife* 2018 Nov 9; **7**.
26. Schmidt EK, Clavarino G, Ceppi M, Pierre P. SUnSET, a nonradioactive method to monitor protein synthesis. Nat Methods. 2009 Apr;6(4):275–7.
27. Yang L, Chen F, Zhu H, Chen Y, Dong B, Shi M, et al 3D genome alterations associated with dysregulated HOXA13 expression in high-risk T-lineage acute lymphoblastic leukemia. Nat Commun

2021 Jun 17; **12**(1): 3708.

28. Love MI, Huber W, Anders S. Moderated estimation of fold change and dispersion for RNA-seq data with DESeq2. Genome Biol. 2014;15(12):550.
29. Yu G, Wang LG, Han Y, He QY. clusterProfiler: an R package for comparing biological themes among gene clusters. OMICS 2012 May; 16(5): 284–287.
30. Keenan AB, Torre D, Lachmann A, Leong AK, Wojciechowicz ML, Utti V, et al. ChEA3: transcription factor enrichment analysis by orthogonal omics integration. Nucleic Acids Res. 2019 Jul;47(W1)(2):W212–24.
31. Garcia-Alonso L, Holland CH, Ibrahim MM, Turei D, Saez-Rodriguez J. Benchmark and integration of resources for the estimation of human transcription factor activities. Genome Res. 2019 Aug;29(8):1363–75.
32. Langmead B, Salzberg SL. Fast gapped-read alignment with Bowtie 2. Nat Methods. 2012 Mar;4(4):357–9.. ; **9**.
33. Li H, Handsaker B, Wysoker A, Fennell T, Ruan J, Homer N, et al The Sequence Alignment/Map format and SAMtools. Bioinformatics 2009 Aug 15; **25**(16): 2078–2079.
34. Faust GG, Hall IM. SAMBLASTER: fast duplicate marking and structural variant read extraction. Bioinformatics 2014 Sep 1; **30**(17): 2503–2505.
35. Wang D, Xiang H, Ning C, Liu H, Liu JF, Zhao X. Mitochondrial DNA enrichment reduced NUMT contamination in porcine NGS analyses. Brief Bioinform 2020 Jul 15; **21**(4): 1368–1377.
36. Yang Y, Fear J, Hu J, Haecker I, Zhou L, Renne R, et al. Leveraging biological replicates to improve analysis in ChIP-seq experiments. Comput Struct Biotechnol J. 2014;9:e201401002.
37. Heinz S, Benner C, Spann N, Bertolino E, Lin YC, Laslo P, et al Simple combinations of lineage-determining transcription factors prime cis-regulatory elements required for macrophage and B cell identities. Mol Cell 2010 May 28; **38**(4): 576–589.
38. Luchtel RA, Bhagat T, Pradhan K, Jacobs WR Jr, Levine M, Verma A, et al. High-dose ascorbic acid synergizes with anti-PD1 in a lymphoma mouse model. Proc Natl Acad Sci U S A. 2020 Jan;21(3):1666–77. ; **117**.
39. Zhu H, Dong B, Zhang Y, Wang M, Rao J, Cui B, et al. Integrated genomic analyses identify high-risk factors and actionable targets in T-cell acute lymphoblastic leukemia. Blood Sci. 2022 Jan;4(1):16–28.
40. Homminga I, Pieters R, Langerak AW, de Rooi JJ, Stubbs A, Verstegen M, et al Integrated transcript and genome analyses reveal NKX2-1 and MEF2C as potential oncogenes in T cell acute lymphoblastic leukemia. Cancer Cell 2011 Apr 12; **19**(4): 484–497.
41. Helsten T, Elkin S, Arthur E, Tomson BN, Carter J, Kurzrock R. The FGFR Landscape in Cancer: Analysis of 4,853 Tumors by Next-Generation Sequencing. Clin Cancer Res 2016 Jan 1; **22**(1): 259–267.

42. Farhan M, Wang H, Gaur U, Little PJ, Xu J, Zheng W. FOXO Signaling Pathways as Therapeutic Targets in Cancer. Int J Biol Sci. 2017;13(7):815–27.
43. Lee TI, Young RA. Transcriptional regulation and its misregulation in disease. Cell 2013 Mar 14; **152**(6): 1237–1251.
44. Costa-Mattioli M, Walter P. The integrated stress response: From mechanism to disease. Science 2020 Apr 24; **368**(6489).
45. Tian X, Zhang S, Zhou L, Seyhan AA, Hernandez Borrero L, Zhang Y, et al. Targeting the Integrated Stress Response in Cancer Therapy. Front Pharmacol. 2021;12:747837.
46. Pakos-Zebrucka K, Koryga I, Mnich K, Ljujic M, Samali A, Gorman AM. The integrated stress response. EMBO Rep. 2016 Oct;17(10):1374–95.
47. Robert F, Williams C, Yan Y, Donohue E, Cencic R, Burley SK, et al. Blocking UV-induced eIF2alpha phosphorylation with small molecule inhibitors of GCN2. Chem Biol Drug Des. 2009 Jul;74(1):57–67.
48. Reid MA, Allen AE, Liu S, Liberti MV, Liu P, Liu X, et al Serine synthesis through PHGDH coordinates nucleotide levels by maintaining central carbon metabolism. Nat Commun 2018 Dec 21; **9**(1): 5442.
49. Lieu EL, Nguyen T, Rhyne S, Kim J. Amino acids in cancer. Exp Mol Med. 2020 Jan;52(1):15–30.
50. Jewell JL, Russell RC, Guan KL. Amino acid signalling upstream of mTOR. Nat Rev Mol Cell Biol. 2013 Mar;14(3):133–9.
51. Babina IS, Turner NC. Advances and challenges in targeting FGFR signalling in cancer. Nat Rev Cancer 2017 May; **17**(5): 318–332.
52. Hoy SM. Pemigatinib: First Approval. Drugs 2020 Jun; 80(9): 923–929.
53. Kang C. Infigratinib: First Approval. Drugs. 2021 Jul;81(11):1355–60.
54. Markham A. Erdafitinib: First Global Approval. Drugs 2019 Jun; 79(9): 1017–1021.
55. Nogova L, Sequist LV, Perez Garcia JM, Andre F, Delord JP, Hidalgo M, et al Evaluation of BGJ398, a Fibroblast Growth Factor Receptor 1–3 Kinase Inhibitor, in Patients With Advanced Solid Tumors Harboring Genetic Alterations in Fibroblast Growth Factor Receptors: Results of a Global Phase I, Dose-Escalation and Dose-Expansion Study. J Clin Oncol 2017 Jan 10; **35**(2): 157–165.
56. Wortel IMN, van der Meer LT, Kilberg MS, van Leeuwen FN. Surviving Stress: Modulation of ATF4-Mediated Stress Responses in Normal and Malignant Cells. Trends Endocrinol Metab. 2017 Nov;28(11):794–806.
57. Gao R, Kalathur RKR, Coto-Llerena M, Ercan C, Buechel D, Shuang S, et al YAP/TAZ and ATF4 drive resistance to Sorafenib in hepatocellular carcinoma by preventing ferroptosis. EMBO Mol Med 2021 Dec 7; **13**(12): e14351.
58. Wei L, Lin Q, Lu Y, Li G, Huang L, Fu Z, et al. Cancer-associated fibroblasts-mediated ATF4 expression promotes malignancy and gemcitabine resistance in pancreatic cancer via the TGF-beta1/SMAD2/3 pathway and ABCC1 transactivation. Cell Death Dis. 2021 Mar;29(4):334. ; **12**.
59. Li C, Wu B, Li Y, Chen J, Ye Z, Tian X, et al Amino acid catabolism regulates hematopoietic stem cell proteostasis via a GCN2-eIF2alpha axis. Cell Stem Cell 2022 Jul 7; **29**(7): 1119–1134 e1117.

60. Hetz C, Papa FR. The Unfolded Protein Response and Cell Fate Control. Mol Cell 2018 Jan 18; **69**(2): 169–181.
61. Luo L, Gribskov M, Wang S. Bibliometric review of ATAC-Seq and its application in gene expression. Brief Bioinform 2022 May 13; **23**(3).
62. Butler M, van der Meer LT, van Leeuwen FN. Amino Acid Depletion Therapies: Starving Cancer Cells to Death. Trends Endocrinol Metab. 2021 Jun;32(6):367–81.
63. Tabe Y, Lorenzi PL, Konopleva M. Amino acid metabolism in hematologic malignancies and the era of targeted therapy. Blood 2019 Sep 26; **134**(13): 1014–1023.
64. Williams RT, Guarecuco R, Gates LA, Barrows D, Passarelli MC, Carey B, et al ZBTB1 Regulates Asparagine Synthesis and Leukemia Cell Response to L-Asparaginase. Cell Metab 2020 Apr 7; **31**(4): 852–861 e856.
65. Zhou X, Zhou R, Rao X, Hong J, Li Q, Jie X, et al. Activated amino acid response pathway generates apatinib resistance by reprograming glutamine metabolism in non-small-cell lung cancer. Cell Death Dis. 2022 Jul;21(7):636. ; **13**.
66. Munde M, Wang S, Kumar A, Stephens CE, Farahat AA, Boykin DW, et al. Structure-dependent inhibition of the ETS-family transcription factor PU.1 by novel heterocyclic diamidines. Nucleic Acids Res. 2014 Jan;42(2):1379–90.
67. Nguyen LV, Caldas C. Functional genomics approaches to improve pre-clinical drug screening and biomarker discovery. EMBO Mol Med 2021 Sep 7; **13**(9): e13189.
68. Ren M, Cowell JK. Constitutive Notch pathway activation in murine ZMYM2-FGFR1-induced T-cell lymphomas associated with atypical myeloproliferative disease. Blood 2011 Jun 23; **117**(25): 6837–6847.
69. Murugan AK. mTOR. Role in cancer, metastasis and drug resistance. Semin Cancer Biol 2019 Dec; 59: 92–111.
70. Chantranupong L, Scaria SM, Saxton RA, Gygi MP, Shen K, Wyant GA, et al The CASTOR Proteins Are Arginine Sensors for the mTORC1 Pathway. Cell 2016 Mar 24; **165**(1): 153–164.
71. Duran RV, Oppliger W, Robitaille AM, Heiserich L, Skendaj R, Gottlieb E, et al Glutaminolysis activates Rag-mTORC1 signaling. Mol Cell 2012 Aug 10; **47**(3): 349–358.
72. Gu X, Orozco JM, Saxton RA, Condon KJ, Liu GY, Krawczyk PA, et al SAMTOR is an S-adenosylmethionine sensor for the mTORC1 pathway. Science 2017 Nov 10; **358**(6364): 813–818.
73. Nicklin P, Bergman P, Zhang B, Triantafellow E, Wang H, Nyfeler B, et al Bidirectional transport of amino acids regulates mTOR and autophagy. Cell 2009 Feb 6; **136**(3): 521–534.
74. Meric-Bernstam F, Larkin J, Tabernero J, Bonini C. Enhancing anti-tumour efficacy with immunotherapy combinations. Lancet 2021 Mar 13; **397**(10278): 1010–1022.
75. Hong M, Clubb JD, Chen YY. Engineering CAR-T Cells for Next-Generation Cancer Therapy. Cancer Cell 2020 Oct 12; **38**(4): 473–488.

76. Zhang S, Gu C, Huang L, Wu H, Shi J, Zhang Z, et al. The third-generation anti-CD30 CAR T-cells specifically homing to the tumor and mediating powerful antitumor activity. Sci Rep. 2022 Jun;21(1):10488. ; **12**.

Figures

Fig.1

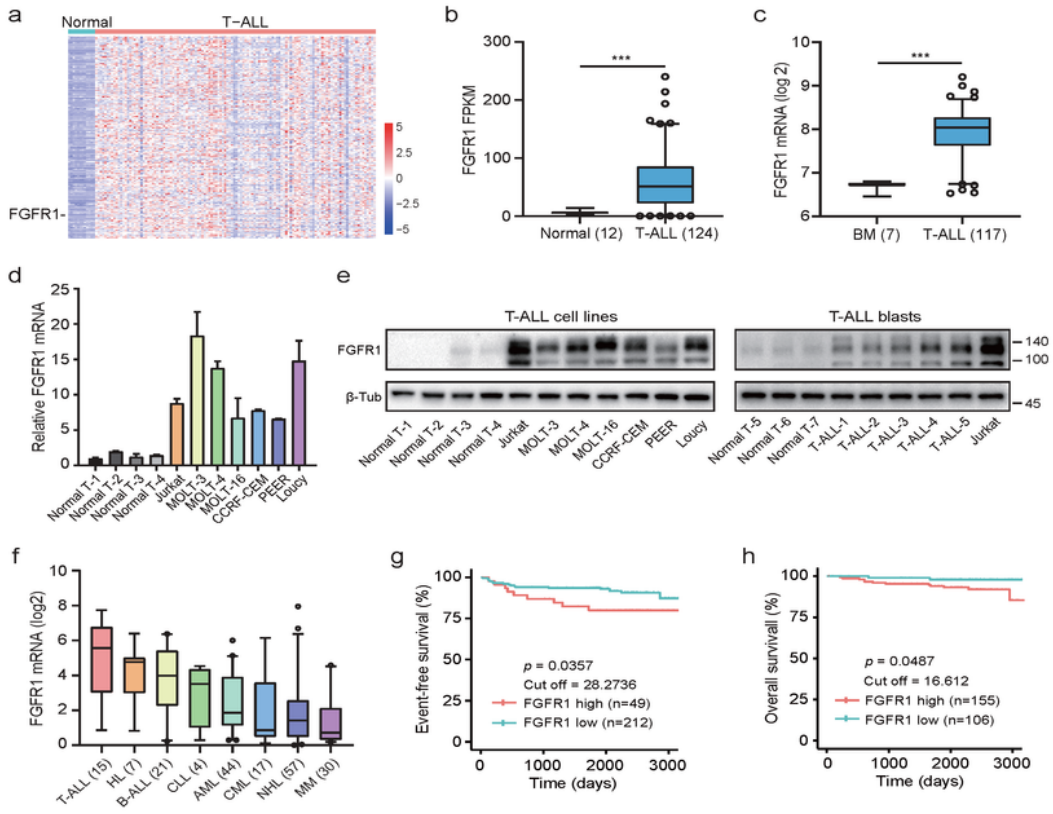

Figure 1

FGFR1 is upregulated in T-ALL and negatively correlated with the prognosis of patients

a Heatmap depicting 226 upregulated expressed genes in a T-ALL cohort (CNCB, HRA000122). Upregulated genes were selected with p <0.05, log2 FoldChange > 50. **b** Fragments Per Kilobase Million (FPKM) of FGFR1 in a T-ALL cohort with 12 normal T cell samples (CNCB, HRA000122). **c** mRNA expression levels of FGFR1 from an RNA-seq data about T-ALL cohort with 7 normal bone marrow samples (GEO, GSE26713). **d** Relative mRNA expression of FGFR1 in T-ALL cell lines and normal T cell samples through qPCR. **e** Protein levels of FGFR1 in T-ALL cell lines (left) and primary T-ALL blasts (right) using western blot, the β-tubulin (β-tub) was used as an internal control. **f** mRNA expression levels of FGFR1 in different hematopoietic malignancies, data from the Cancer Cell Line Encyclopedia (CCLE). **g** Event-free survival of T-ALL patients with higher or lower expression of FGFR1, data from TARGET, phs000464. **h** Overall survival of T-ALL patients with higher or lower expression of FGFR1, data from TARGET, phs000464. Data are mean ± SD (Two-tailed unpaired Student's t test, *** p< 0.001).

Fig.2

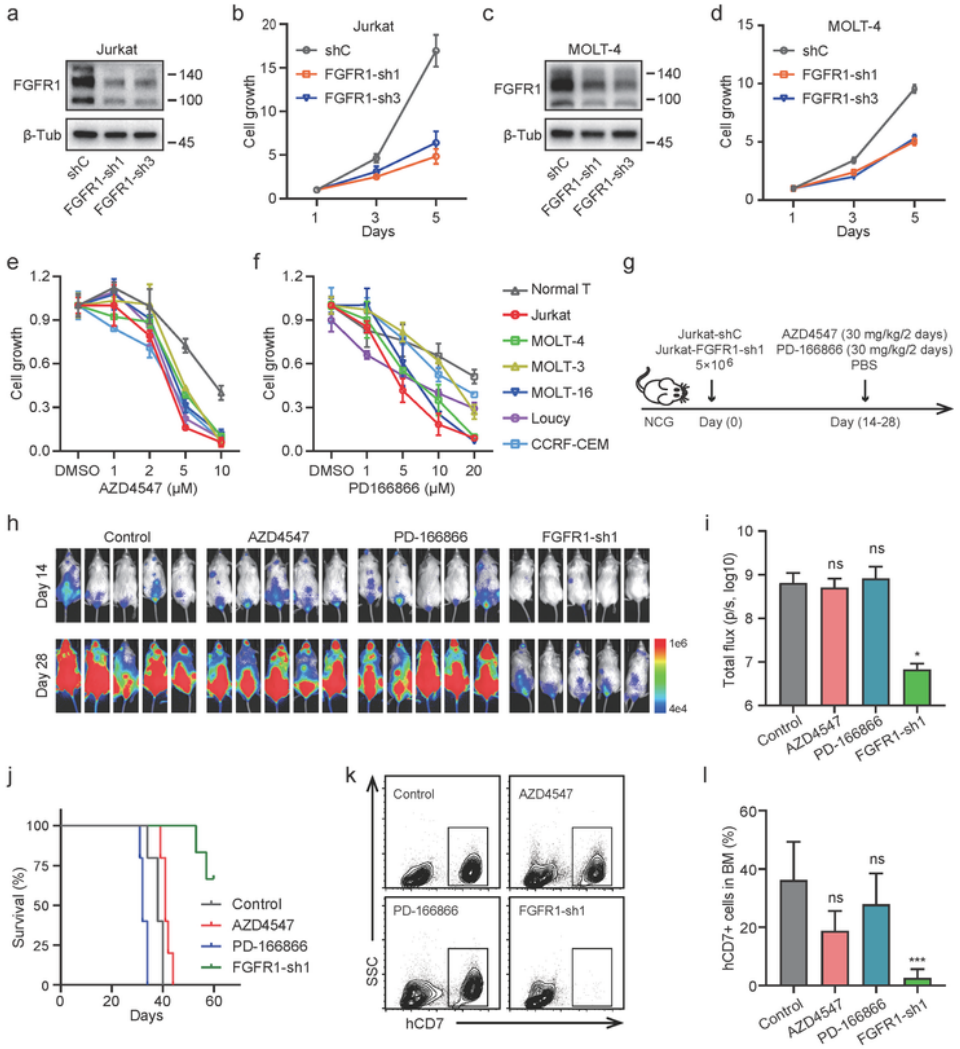

Figure 2

FGFR1 is a potential therapeutic target in T-ALL but leukemia cells are resistant to FGFR1 inhibitors

a, c The knockdown efficiency of FGFR1 in (**a**) Jurkat or (**c**) MOLT-4 cells. Cells were harvested at 72 h after transfection using lentivirus vectors, non-target lentivirus vector (shC) was used as the negative control. **b, d** Relative cell growth of (**b**) Jurkat or (**d**) MOLT-4 cells after FGFR1 knockdown, cell counting

was performed on day 1, 3, and 5 respectively. **e, f** The relative cell growth of T-ALL cell lines and normal T cell, cell counting was performed at 72 h after treatment with different concentration gradients of FGFR1 inhibitors (**e**) AZD4547, and (**f**) PD-166866. **g-i** Jurkat cell-derived xenograft (CDX) experiment in NCG mice, 5×10^6 luciferase labeled FGFR1 knockdown Jurkat cells (Jurkat-FGFR1-sh1) or knockdown control Jurkat cells were injected through the tail vein, AZD4547 (30 mg/kg/2 days) or PD-166866 (30 mg/kg/2 days) was intraperitoneally administrated from day 14 to day 28, the control group was treated with PBS. (**g**) Schematic outline of cell-derived xenograft (CDX) (**h**) Bioluminescent imaging of cell-derived xenograft (CDX). (**i**) Total photon flux of bioluminescent at day 28. (**j**) Kaplan-Meier survival curves of Jurkat cell-derived xenograft mice (CDX). The endpoint was that weight loss exceeded 20% of the body weight of a similar normal animal according to guidelines of the Canadian Council on Animal Care (CCAC). (**k**) Analysis of bone marrow invasion by using anti-human CD7 antibody through flow cytometry. (**l**) Quantification of bone marrow invasion. Data are mean ± SD (Two-tailed unpaired Student's t test, * $p < 0.05$, *** $p < 0.001$, ns = no significance).

Fig.3

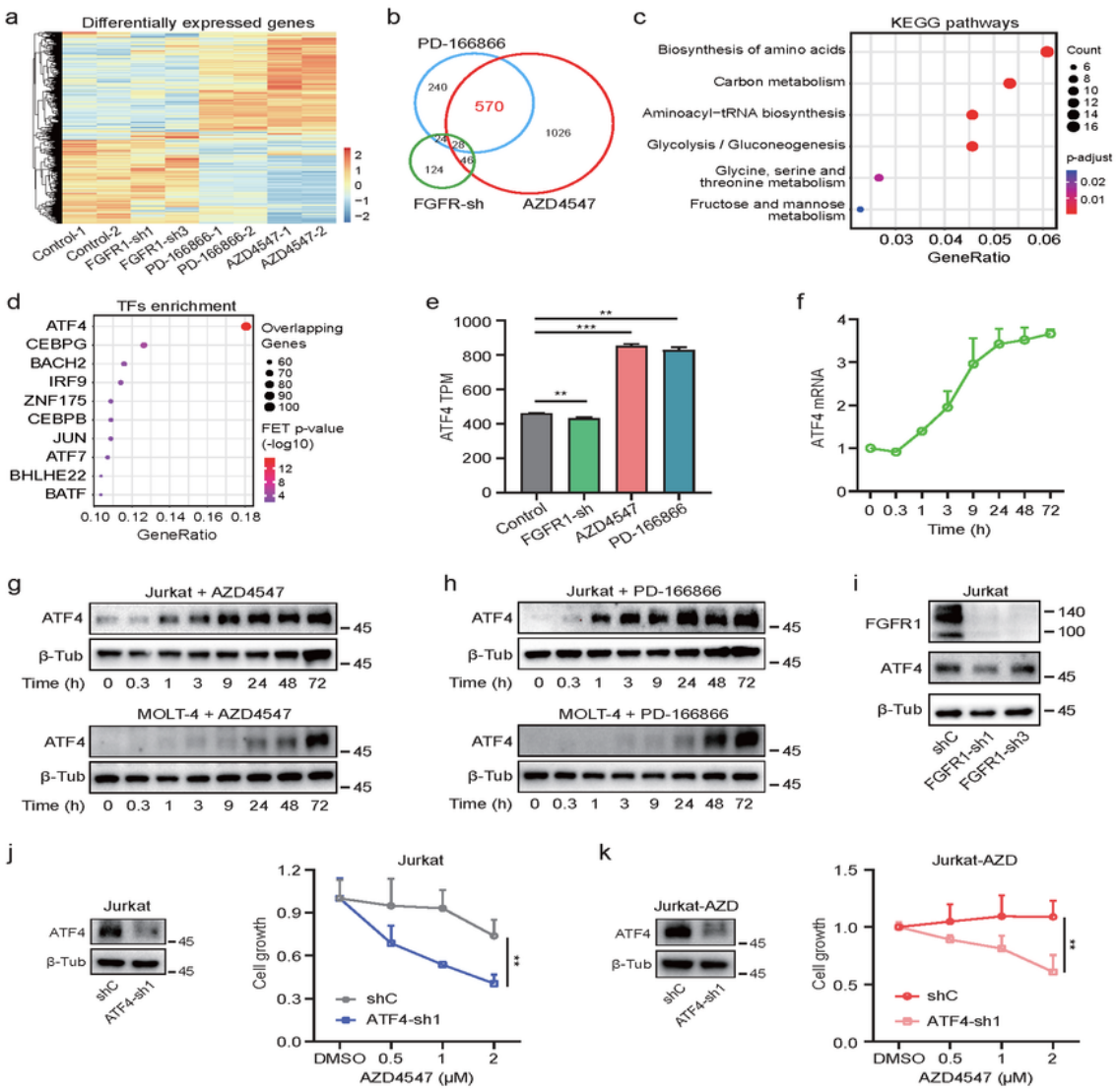

Figure 3

ATF4 is essential for the resistance of T-ALL against FGFR1 inhibitors

a Heatmap of the differentially expressed genes (DEGs) in groups of FGFR1-sh, AZD4547, and PD-166866 compared with the group of control through RNA-seq analysis. DEGs were filtrated with $p < 0.05$ and $|\log 2\ FoldChange| > 0.5$. The color indicates the *Z*-score of different genes expression. **b** Venn

diagram depicting the number of DEGs shared in different groups. **c** KEGG pathway analysis of 570 common DEGs that were shared in both AZD4547 and PD-166866 treatment groups. **d** Transcription factors enrichment analysis of 570 common DEGs that shared in both AZD4547 and PD-166866 treatment groups **e** TPM of ATF4 in different groups based on RNA-seq data. **f** Time series analysis of the mRNA levels of ATF4 in Jurkat exposed to AZD4547 (2 μM) through qPCR. **g, h** Time series analysis of the protein levels of ATF4 in Jurkat (up) or MOLT-4 (down) exposed to (**g**) AZD4547 (2 μM) and (**h**) PD-166866 (4 μM). the β-tubulin (β-tub) was used as the internal control **i** The protein levels of FGFR1, and ATF4. Jurkat cells were harvested at 72 h after transfected with FGFR1 knockdown (FGFR1-sh1, and FGFR1-sh3) or non-target lentivirus vectors (shC), the β-tubulin (β-tub) was used as the internal control. **j, k** The protein levels of ATF4 (left) and relative cell growth of (**j**) Jurkat cells and (**k**) the more resistant Jurkat cells (Jurkat-AZD). Cells were treated with different concentrations of AZD4547 and cell counting was performed at 72 h after treatment. Data are mean ± SD (Two-tailed unpaired Student's t test, ** $p < 0.01$, ns = no significance).

Fig.4

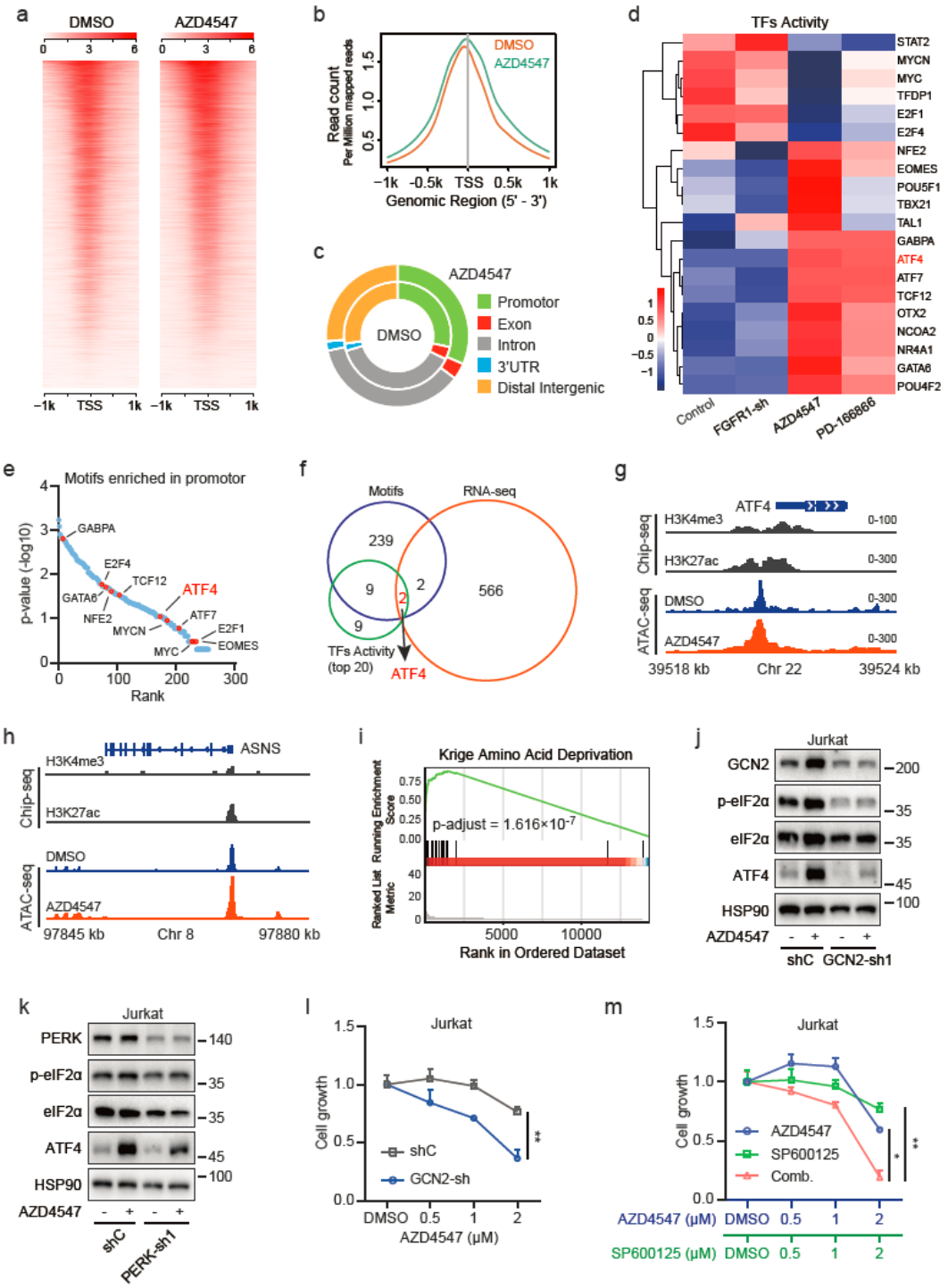

Figure 4

Expression of ATF4 is stimulated by increased chromatin accessibility combined with GCN2-mediated translational activation

a Average ATAC-seqsignal and **b** quantification of average ATAC-seq signal around transcription start site (TSS) in Jurkat cells after 96 h with AZD4547 (2 μM) treatment, DMSO was used as the control. **c**

Distribution of ATAC-seq signal in promotor, exon, intron, 3'UTR, and distal intergenic. **d** Top 20 significantly activated transcription factors (TFs) in each group based on RNA-seq data, the color indicates *Z*-scaled average TFs activity score. **e**Rank of motifs enriched in the region of promotor based on ATAC-seq. **f**Venn diagram depicting the number of common genes in different groups. the "Motifs" was the group of motifs enriched in promotor, the "RNA-seq" was the group of 570 common DEGs shared in both AZD4547 and PD-166866 groups based on RNA-seq data, the "TFs activity (Top 20)" was the group of top 20 differentially activated TFs. **g** Signal of Chip-seq and ATAC-seq around the chromosomal region of ATF4. **h**Signal of Chip-seq and ATAC-seq around the chromosomal region of ASNS. **i**Gene Set Enrichment Analysis (GSEA) of 570 common DEGs shared in both groups of AZD4547 and PD-166866. **j, k** The protein levels of GCN2, p-eIF2α, eIF2α, ATF4 in Jurkat cells with (**j**) GCN2 knockdown and (**k**) PERK knockdown. Cells were harvested after 72 h with GCN2-sh1 or PERK-sh1 or non-target lentivirus vector transfection (shC) and 6 h treatment with AZD4547 (2 μM) or DMSO. HSP90 was used as the internal control. **l** Relative cell growth of GCN2 knockdown Jurkat cells compared with control Jurkat cells (shC), cell counting was performed at 72 h after AZD4547 treatment. **m** Relative cell growth of Jurkat cells treated with AZD4547 combined SP600125. Cell counting was performed at 72 h after treatment. Data are mean ± SD (Two-tailed unpaired Student's t test, * $p < 0.05$, ** $p < 0.01$).

Fig.5

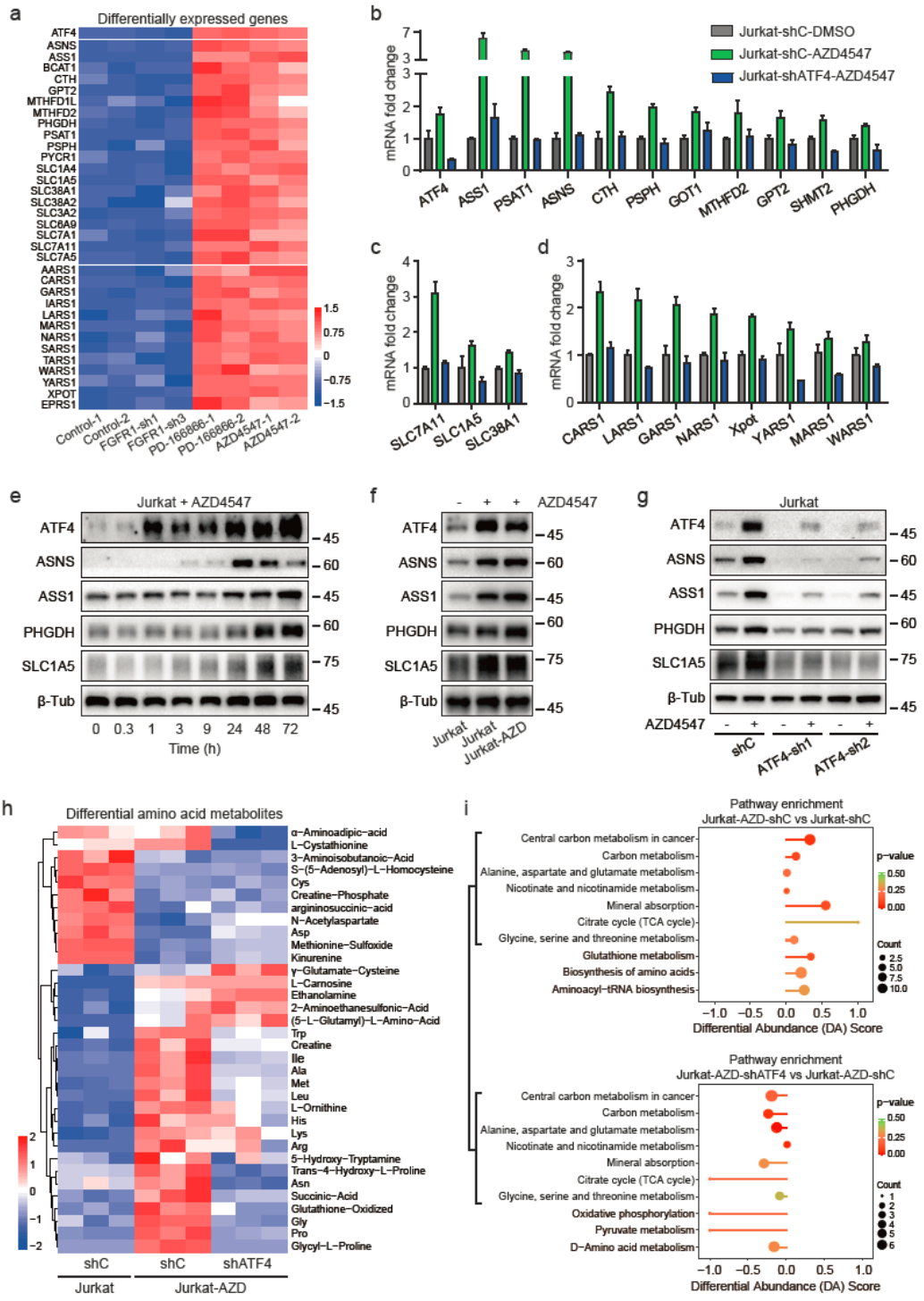

Figure 5

ATF4 is a crucial initiatorto upregulate the metabolic genes and remodel the amino acid metabolism

a Heatmap depicting the differentially expressed genes (DEGs) about metabolism based on RNA-seq data. The color indicates the *Z*-score of different genes expression. **b-d** Relative mRNA levels of DEGs in the group of (**b**) typical kinases, (**c**) transporters, and (**d**) aminoacyl-tRNA biosynthesis after ATF4

knockdown and AZD4547 treatment. Jurkat cells were harvested for qPCR analysis at 48 h after AZD4547 (2 μM) treatment. **e** Time series analysis of protein levels of ATF4, ASNS, ASS1, PHGDH and SLC1A5 in Jurkat cells exposed to AZD4547 (2 μM). The β-tubulin (β-tub) was used as the internal control. **f** Protein levels of ATF4, ASNS, ASS1, PHGDH, and SLC1A5 in Jurkat and the more resistant Jurkat cells (Jurkat-AZD) with or without AZD4547 (2 μM) treatment for 48 h. **g** The protein levels of ATF4, ASNS, ASS1, PHGDH and SLC1A5 in ATF4 knockdown Jurkat cells (ATF4-sh1, ATF4-sh2), non-target lentivirus vector (shC) was used as the control, the cells were harvested at 48 h after AZD4547 (2 μM) treatment. **h**Differential amino acid metabolites of different groups through targeted metabolomics analysis. The Jurkat cells were harvested after 48 h of transfection. The color indicates the *Z*-score of the quantity of metabolites. **i** Pathway analysis of the differential amino acid metabolites. Differential abundance score depicting the average, gross transformations of all metabolites in each pathway. the score of 1 indicates all measured metabolites increase in the pathway, and -1 indicates all measured metabolites decrease in the pathway. Data are mean ± SD.

Fig.6

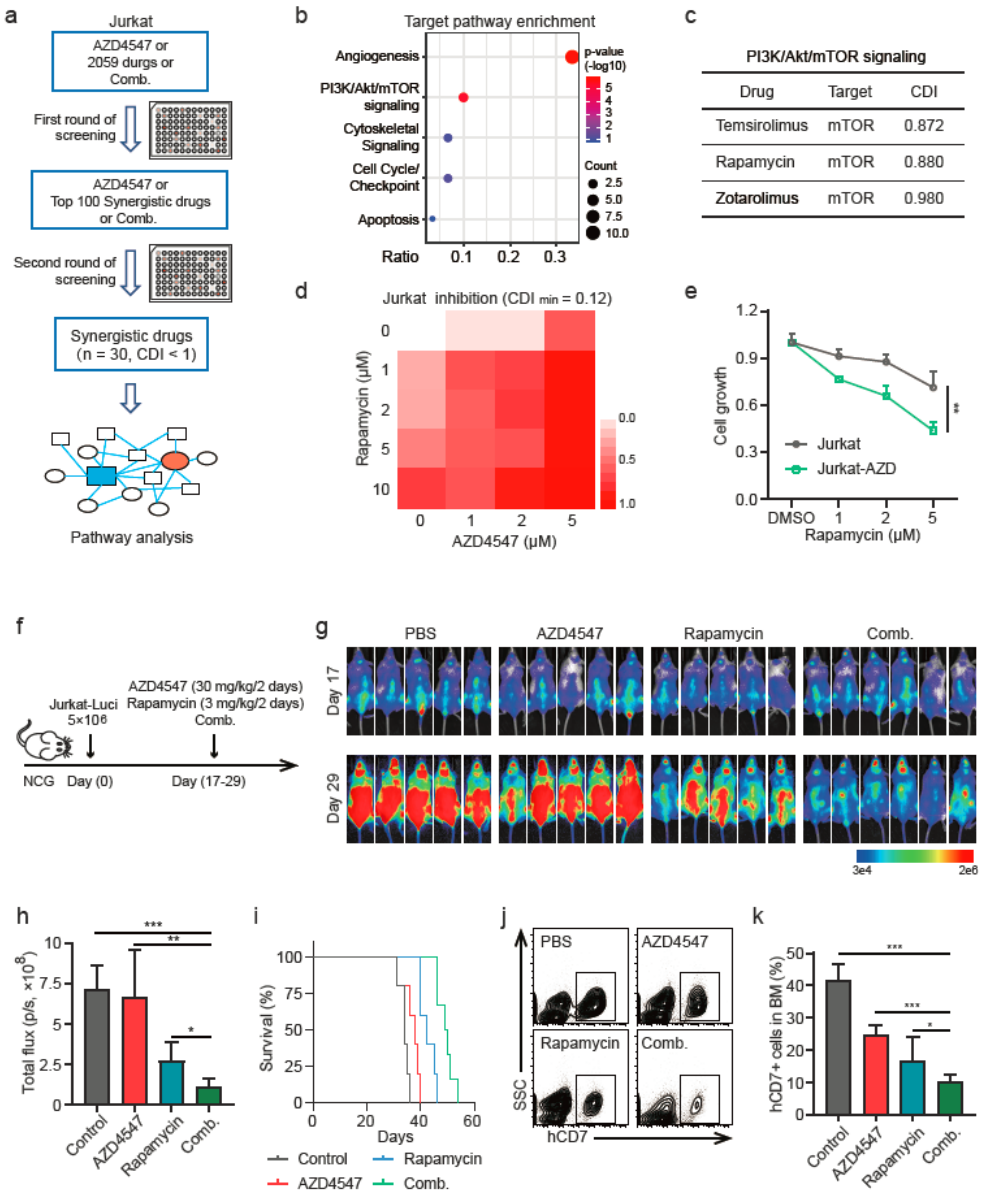

Figure 6

Targeting mTOR could overcome the resistance against FGFR1 inhibitors

a Schematic of drug screening that AZD4547 combined with 2059 approved drugs. The Jurkat cells were treated with AZD4547 (2 μM) or each drug or a combination of these two drugs for 72 h, Cell viability was detected using CCK-8 kit. The synergistic efficiencies were calculated using the coefficient of drug

interaction (CDI), CDI < 1 indicated a synergistic effect. **b** The target pathways enrichment analysis of 30 synergistic drugs. **c** List of drugs enriched in PI3K/Akt/mTOR signaling. **d** Synergistic inhibition of AZD4547 and Rapamycin in Jurkat cells. The cell counting was performed at 72 h after AZD4547 and Rapamycin treatment. **e** Relative cell growth of Jurkat and the more resistant Jurkat cells (Jurkat-AZD) exposed to Rapamycin for 72 h. **f-k** Jurkat cell-derived xenograft (CDX) experiment in NCG mice, 5×10^6 luciferase labeled Jurkat cells were injected through the tail vein, AZD4547 (30 mg/kg/2 days) or PD-166866 (30 mg/kg/2 days) or combination of these two inhibitors was intraperitoneally administrated from day 17 to day 29, the control group was treated with PBS. (**f**) schematic of cell-derived xenograft (CDX) (**g**) Bioluminescent imaging of Jurkat-derived xenograft mice. (**h**) Total photon flux of bioluminescent of Jurkat-derived xenograft mice at day 29. (**i**) Kaplan-Meier survival curves of Jurkat-derived xenograft mice in different groups. The endpoint was that weight loss exceeded 20% of the body weight of a similar normal animal according to guidelines of the Canadian Council on Animal Care (CCAC). (**j**) Analysis of bone marrow invasion using anti-human CD7 antibody through flow cytometry. (**k**) Quantification of bone marrow invasion in different groups. Data are mean ± SD (Two-tailed unpaired Student's t test, * $p < 0.05$, ** $p < 0.01$, *** $p < 0.001$).

Fig.7

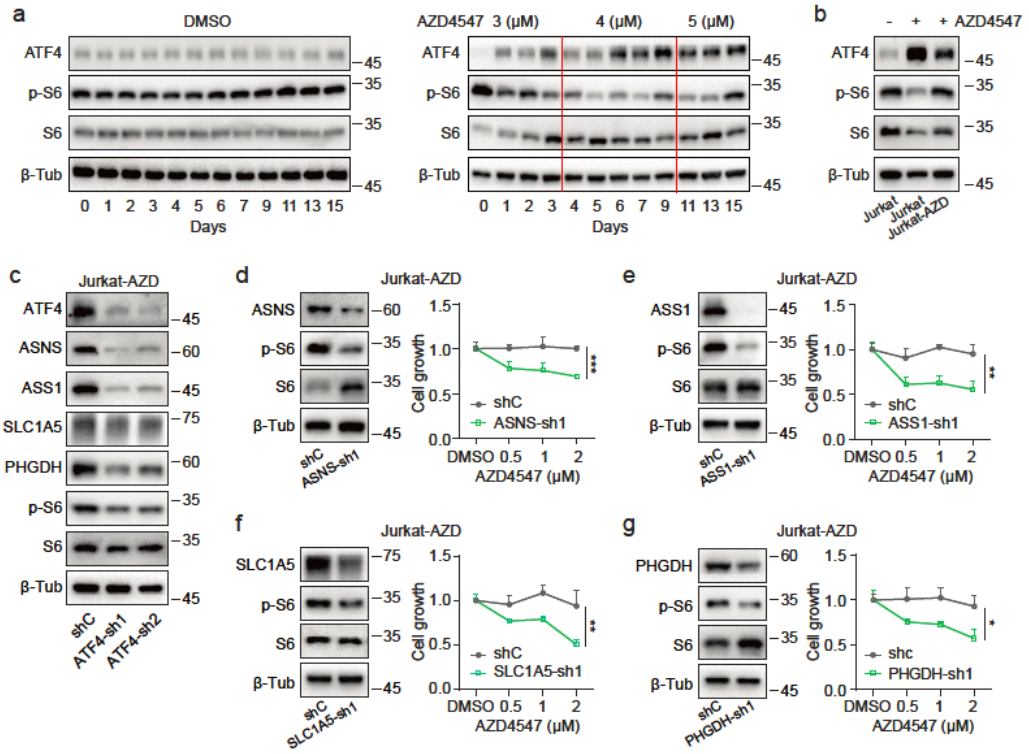

Figure 7

The enhanced amino acid metabolism induced the activation of mTORC1

a Time series analysis of protein levels of ATF4, the phosphorylation levels of S6 and ribosomal protein S6 (S6) in Jurkat cells after AZD4547 treatment (right). DMSO was used as control (left). **b** Protein levels of ATF4, the phosphorylation levels of S6 and S6 in Jurkat or the more resistant Jurkat (Jurkat-AZD) cells

with or without AZD4547 (2 μM), the β-tubulin (β-tub) was used as the internal control. **c** Protein levels of ATF4, ASS1, ASNS, PHGDH, SLC1A5 and phosphorylation level of S6 in ATF4 knockdown Jurkat cells. The cells were harvested at 72 h after ATF4 knockdown lentivirus vectors transfection, the β-tubulin (β-tub) was used as the internal control. **d-g** Protein levels of the S6 and phosphorylation level of S6 (left) and relative cell growth (right) in the more resistant Jurkat (Jurkat-AZD) cells. after (**d**) ASNS knockdown, (**e**) ASS1 knockdown, (**f**) SLC1A5 knockdown, or (**g**) PHGDH knockdown. Total proteins were harvested at 72 h after lentivirus vectors transfection, and the cell counting was performed at 72 h after different concentrations of AZD4547. Data are mean ± SD (Two-tailed unpaired Student's t test, * $p < 0.05$, ** $p < 0.01$, *** $p < 0.001$).

Supplementary Files

This is a list of supplementary files associated with this preprint. Click to download.

- Schematic.png
- ZhangZ.etalSupplementaryFigure15.pdf
- ZhangZ.etalSupplementaryFigurelegends.docx
- ZhangZ.etalTablesS1S4.xlsx